Investigation on conductivity and optical properties for blend electrolytes based on iota-carrageenan and acacia gum with ethylene glycol

M. Nandhinilakshmi[1], D. Vanitha[2,*] , N. Nallamuthu[2], K. Sundaramahalingam[3], and P. Saranya[1]

[1] *Multi-Functional Materials Laboratory, International Research Centre, Kalasalingam Academy of Research and Education, Krishnankoil, Virudhunagar, Tamil Nadu 626 126, India*

[2] *Department of Physics, Kalasalingam Academy of Research and Education, Krishnankoil, Virudhunagar, Tamil Nadu 626 126, India*

[3] *Department of Physics, Arulmigu Kalasalingam College of Arts and Science, Krishnankoil, Virudhunagar, Tamil Nadu 626 126, India*

ABSTRACT

Iota-carrageenan (IC) and Acacia gum (AG)-blended biopolymer electrolytes are prepared by solution casting method. Then various percentages of ethylene glycol (EG)-added blend electrolytes are also prepared. X-ray diffraction studies are used to investigate the amorphous nature of plasticizer-added biopolymer electrolyte. The functional groups and the formation of complexes between polymer chains and plasticizer are discovered by Fourier transform infrared analysis. The dielectric behavior is measured by using an AC impedance analyzer at various temperatures (303–373 K) and frequencies (1 Hz to 1 MHz). The conductivity is improved by the addition of plasticizer and increase in temperature. For 0.75 ml of EG-added electrolyte, the highest conductivity of 2.96×10^{-4} S cm^{-1} is obtained. The Arrhenius relation is used to determine the temperature dependence of conductivity of polymer electrolyte films. The minimum activation energy of 0.06 eV is found for 0.75 ml EG-added sample. The tangent loss peak seen at 303 K is used to determine relaxation time (τ). The non-Debye character of the electrolytes is shown by the modulus spectra. The relaxation process is studied using the Argond plot. The optical characteristics of UV irradiation are analyzed. Cyclic voltammetry and linear sweep voltammetry are used to confirm electrochemical stability of plasticizer-added solid polymer electrolytes.

Address correspondence to E-mail: vanibala2003@gmail.com

1 Introduction

The last two decades confront the high-energy requirement for further development and technological improvement. Fuel cells, electric double-layer capacitors, sensor and battery cells are drawing significant roles as alternative energy storage devices throughout the whole range of electrical and thermal energy applications. The battery consists of three divisions that are two electrodes sandwiched with electrolyte. Liquid electrolytes have been replaced with solid polymer electrolytes (SPEs) as a result of unsteady electrochemical performance, spilling unsafe, corrosion, and low range of ion selectivity [1, 2].

Compared with synthetic polymers, polyethylene oxide (PEO), poly(vinylidene fluoride) (PVdF), polyvinyl alcohol (PVA), polyacrylonitrile (PAN) are the natural polymers which are abundant in nature and it is having biocompatibility, renewable, and cost-effective properties. The usage of biodegradable polymers as a host can diminish environmental waste because they are renewable and eco-friendly [3]. Synthetic polymers have disadvantages such as unfavorable property of crystallinity for achieving high ionic conductivity, high cost, toxic, and non-biodegradable in nature. These are the main reason to work with eco-friendly polymer. Some of the host biopolymers used in electrolytes are starch [3, 4], pectin [5], chitosan [6], agar–agar [7], protein [8], iota-carrageenan, IC [9], kappa-carrageenan [10], cellulose acetate, carboxymethyl derivatives [11], and carboxymethyl cellulose [12, 13].

Among these polysaccharides which are extracted from red seaweed species of the class, Rhodophyceae-carrageenan is water soluble. Based on the different positions and numbers of an ester sulfate group in the structure of Carrageenan, it is divided into three types known as Kappa [14], Iota [15], and Lambda. The K- and I-carrageenans are known as gel-forming [16] carrageenans, whereas λ-carrageenan is a thickener or viscosity builder [17]. Iota-carrageenan consists of β-υ-galactopyranose and α-υ-galactopyranose monomers linked by α-(1 → 3) and β-(1 → 4) glycosidic bridges, comparing with other carrageenans. Iota-carrageenan has flexibility nature [18]. From literature review, minimum work is available in IC with blend polymer. IC blend with chitosan, poly(ethylene glycol) (PEG), and H_3PO_4

(*ortho*phosphoric acid)-added electrolyte has reported the conductivity of 6.29×10^{-4} S cm^{-1} [18].

Polysaccharides also include gums taken from plants, animals, marine, and microbial sources. Most available gums tend to form gels by adding water [19]. Several types of gums are Acacia gum, AG [20], Guar gum [21], Tragacanth gum [22], Gellan gum [23], Moringa gum [24], and Xanthan gum [19]. AG, which is also known as Gum Arabic, refers to the tree gum exudate of the Acacia tree. It is a highly branched polysaccharide and contains glycoprotein components. Gum Arabic is abundantly available and primarily used as an emulsifier, stabilizer, and thickening agent [2]. To enhance ionic conductivity blend polymer techniques approach good result. Thus the IC blend with AG work was carried to this manuscript.

Plasticization is one of the current ways often performed to resolve the low conductivity issue in the biopolymer electrolyte (BPEs) system using several plasticizers, according to previous study [25–27]. Plasticizers could penetrate and increase the distance among molecules while decreasing the polar groups of polymer and produce the smooth texture, more flexible and enhancing the chemical and mechanical stability of membranes [28–30].One of the main aims in polymer electrolyte research is to develop polymeric systems with high ionic conductivity, in addition to their potential application in electrochemical devices.

Recent research report that IC-based electrolyte attains 3.57×10^{-4} S cm^{-1} conductivity value with lithium salt and plasticizer [31]. Earlier literature survey explained the minimum report in AG with blend polymers. AG blends with PVA, furthermore 0.5 g (20 wt%) of formaldehyde as a cross linker and 1 g (40 wt%) of glycerol electrolyte report 2.22×10^{-5} S cm^{-1} conductivity value [32]. AG was combined with PVA, as well as 0.5 g (20 wt%) formaldehyde as a crosslinker, 1 g (40 wt%) glycerol, and LiClO$_4$ as an electrolyte. The conductivity value is 1.64×10^{-4} S cm^{-1} [33].

2 Materials

The polymers, the monomer of IC with high molecular weight of 946.8 g mol^{-1} with 99% purity, and 92 g mol^{-1} molecular weight of AG with SQ grade were obtained from HiMedia chemicals (HiMedia

Laboratories Pvt. Ltd.) and Qualigens Fine Chemicals Pvt. Ltd respectively. Ethylene glycol (EG) with molecular weight of 62.07 g mol^{-1} having 99% purity (GC) was purchased from Merck Specialities Private Limited. Throughout the preparation, deionized water was used as the solvent.

3 Characterization techniques

The phase structure of the polymer electrolyte has been confirmed with an instrument Bruker made X-ray diffractometer. This device was scanned with CuKα radiation at a rate of 5° min^{-1} in the range of $2\theta = 10°$ to 60°. The Shimadzu IR Tracer 100 spectrometer is used to observe FTIR spectra at wavenumber from 4000 to 400 cm^{-1} with a resolution of 4 cm^{-1}. The ionic conductivity and dielectric study of the polymer electrolytes have been carried out using a computer-controlled Hioki 3532-50 LCR Hitester over a frequency range of 42 Hz to 1 MHz in the temperature range of 303–368 K. Optical properties were carried out by Beckman DU640 UV/Vis spectrophotometer. The electrochemical property of the sample was investigated by cyclic voltammetry (CV) using CH-Instrument Model 6008e.

3.1 Experimental details

Synthesis of IC and AG unification electrolyte was prepared by using the solution casting method. The optimized blend ratio 60 wt% (0.94 g) of IC solution was made by dissolving the polymer in 40 ml of deionized water at 60 °C for 3 h and 40 wt% (0.06 g) of AG solution (IAG) was made separately in 20 ml of deionized water and stirred at room temperature for 3 h. To achieve a clear solution, progressively mix these two solutions and then stir for 3 h. After that, a variable quantity such as 0.25 ml, 0.75 ml, and 1.25 ml (IAG01, IAG02, and IAG03) of C$_2$H$_6$O$_2$ (EG) was added as a plasticizer, and the mixture was stirred for 12 h. Finally, the transparent solution was casted into a petri dish and placed in the oven at 70 °C for a dry process. The prepared electrolytes had attained 0.15 mm to 0.32 mm thickness. The picture of the prepared electrolyte and the preparation technique flowchat is given in Fig. 1a, b.

# 4 Results and discussion

4.1 XRD

XRD analysis helps to discuss the amorphous nature by the absence of intense peaks. X-ray diffraction pattern of pure IC (ICP), Gum acacia pure (AGP), IC blend Gum acacia (IAG), and different amounts of EG-added system (IAG01, IAG02, IAG03) is shown in Fig. 2. ICP electrolyte has intense humps at $2\theta = 20°$, 30°, and 41° [34]. AGP electrolyte shows humps at $2\theta = 20°$, 40° and the humps that appear in blend electrolyte IAG confirms the presence of IC and gum acacia in the system. The different amounts of EG-added system show amorphous nature like ICP electrolyte as well as the hump also appears in IAG01, IAG02, and IAG03. The amorphous nature and the density of charge carriers increase simultaneously as EG concentration increases, which probably helps in enhancing the conductivity of the polymer electrolytes. However, in IAG02 electrolyte humps were observed with a slight decrease in intensity [35]. It confirms that the addition of EG helps to structure rearrangement and there is an interaction between polymer and EG in the biopolymer electrolyte [36].

4.2 FTIR

The FTIR analysis examines the interactions between IC and AG blend by investigating the variations in the wavenumber, peak location of the functional group is shown in Fig. 3. The observed vibrational bands are listed in Table 1. The vibrational peaks are at 914 cm^{-1} corresponding to C–O–C of 3–6 anhydrogalactose stretching. It confirms the galactose present in pure IC electrolyte [37]. This band is shifted to 920 cm^{-1} for blend electrolyte sample (IAG) and plasticizer-added samples (IAG01, IAG02, and IAG03). The wavenumber peak at 738 cm^{-1} represents sulfate C-4 galactose stretching of IC in IAG, IAG01, IAG02, and IAG03 samples. The band located at 839 cm^{-1} is due to –O–SO$_3$ stretching at D-galactose-4-sulfate of IC. There are noticeable changes with the decrease of transmittance (%) value rather than wavenumber. This confirms the incorporation of EG in the blend electrolytes.

For pure AG electrolyte (AGP), there exhibits a vibrational peak at 1016 cm^{-1} corresponding to C–O stretching which is shifted to 974 cm^{-1} and 977 cm^{-1}

Fig. 1 a The flowchart for the preparation of polymer blend electrolyte. **b** Prepared polymer electrolyte
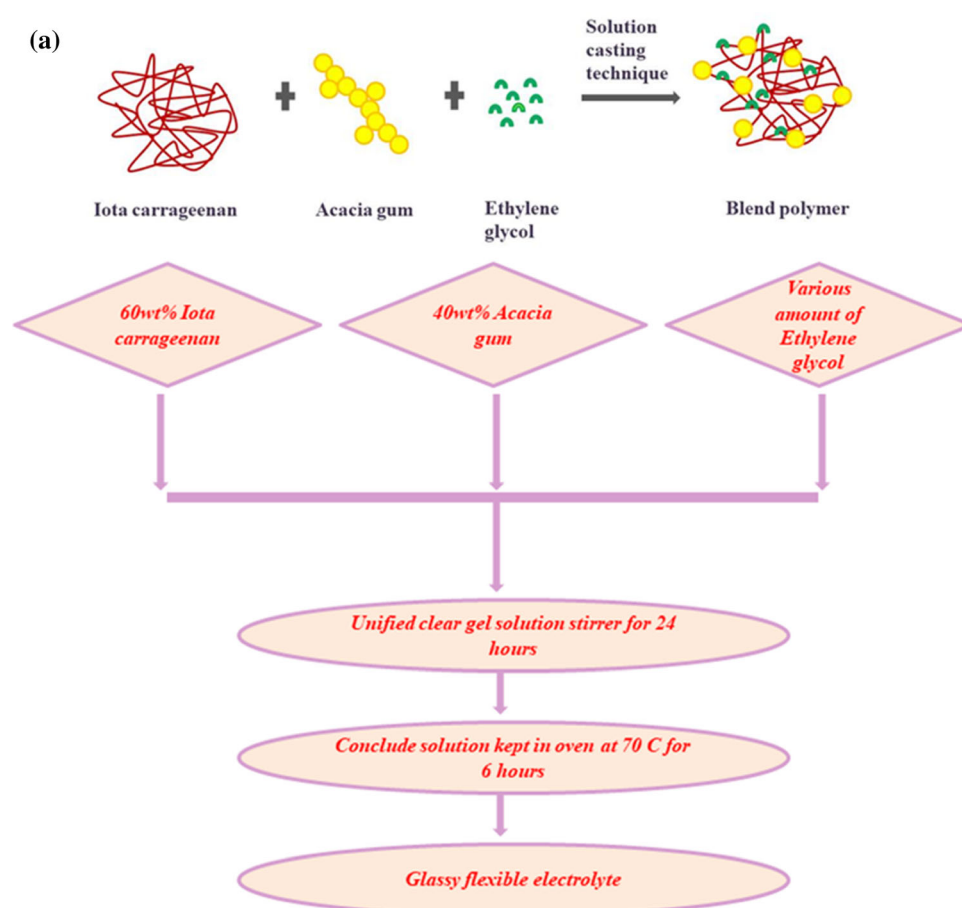
for blend sample and plasticizer-added samples. The band at 1425 cm^{-1} present in AGP indicates the symmetrical and asymmetrical vibration of –COO$^-$ group in the electrolyte [38]. In all blend electrolyte system, this band is observed at 1438 cm^{-1}. The hydroxyl group OH, C–H, and O–H water deformation band has been ascribed to broadband at 3302 cm^{-1}, 2891 cm^{-1}, and 1610 cm^{-1}. It reveals the presence of AG in blend system [39]. These bands are shifted to 3358 cm^{-1}, 2926 cm^{-1}, and 1633 cm^{-1} for
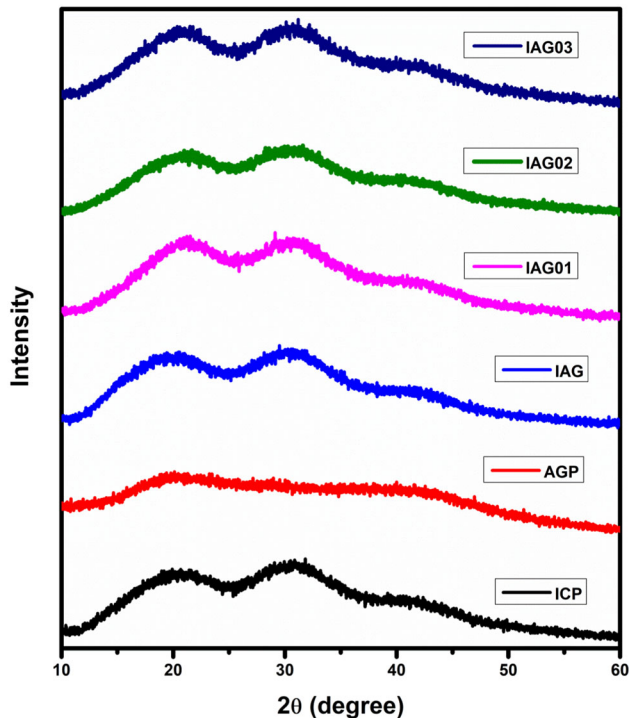
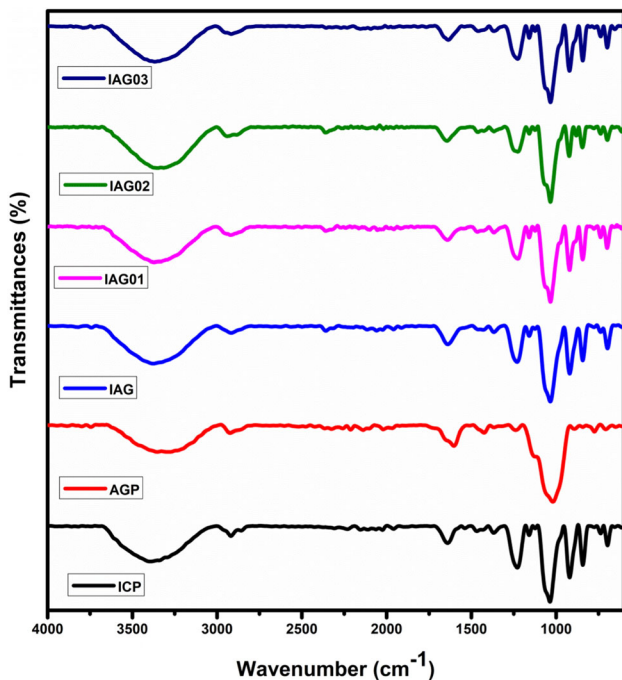**Fig. 2** X-ray diffraction pattern of the prepared electrolyte

Fig. 3 Fourier transform infrared spectra of ICP, AGP, IAG, IAG01, IAG02, and IAG03

blend polymer electrolyte (IAG). The OH group is shifted to 3361 cm^{-1}, 3323 cm^{-1}, and 3354 cm^{-1} for EG-added electrolytes. This confirms the hydroxyl

group in EG incorporated with blend polymer electrolyte. The O–H water deformation band was observed at 1639 cm^{-1}, 1641 cm^{-1}, and 1635 cm^{-1} in IAG01, IAG02, and IAG03. In plasticizer-added system, C–H band is observed at 2932 cm^{-1}. The vibrational band of S–O sulfate stretching and CH$_2$ asymmetric stretching of IC is observed at 1228 cm^{-1} and 1033 cm^{-1} and this band is shifted to 1236 cm^{-1} and 1031 cm^{-1} for IAG. The changes in wavenumber of S–O sulfate stretching for EG-added samples are located at 1238 cm^{-1}, 1232 cm^{-1}, and 1224 cm^{-1}. The band of CH$_2$ asymmetric stretching is observed at 1032 cm^{-1} for IAG01, IAG02, and IAG03 samples [40].

4.3 Cole–Cole plot

Using the AC impedance spectroscopy, the electrical characterization for the prepared electrolytes has been performed. Nyquist plots for the prepared sample are shown in Fig. 4. Cole–Cole plot in Fig. 4a, c shows the spike at a lower frequency which is caused by the effect of polarization then a small semicircle present at high-frequency region due to bulk resistance effect. Figure 4b represents the plot for Pure Gum Acacia, there is a Semicircle at the higher frequency which represents the bulk effect.

The Nyquist plots for the blend of IAG and different amounts of EG with the blend IAG are represented in Fig. 4c, d. Nyquist plot of IAG03 blend polymer electrolyte has two semicircles followed with the spike. The two semicircles represent the two parallel combinations of bulk resistance with QPE [13].

The Cole–Cole plot for the samples IAG01 shows the very small semicircle followed with spike at the lower frequency by the polarization effect and denotes the parallel combinations of bulk resistance and QPE. The sample IAG02 shows a low-frequency spike and the equivalent circuit is the series combination of resistance and QPE. From this present study, the obtained bulk resistance value is calculated by the ZSimpWin Software and is shown in Table 2. The ionic conductivity of the prepared SPE samples is calculated by using the below equation,

$$\sigma = \frac{l}{AR_b} \, \text{Scm}^{-1}. \tag{1}$$

Here, "l" denotes the thickness of the sample and "A" represents the area of the sample. And R_b is the

Table 1 Functional group assignments for ICP, AGP, IAG, IAG01, IAG02, and IAG03

| Assignment	Wave number (cm^{-1})					
	ICP	AGP	IAG	IAG01	IAG02	IAG03
O–H stretching	3395	3302	3358	3361	3323	3354
C–H stretching	2897	2891	2926	2932	2932	2932
H–O–H (water deformation band)	1641	1610	1633	1639	1641	1635
–COO$^-$ symmetrical and asymmetrical stretching	1436	1425	1438	1438	1438	1438
S–O sulfate stretching	1228	–	1236	1238	1232	1224
CH$_2$ asymmetric stretching	1033	–	1031	1032	1032	1032
C–O stretching	1060	–	1064	1064	1064	1064
C–O stretching	–	1016	974	977	977	977
C–O–C of 3–6 anhydro-galactose stretching	914	–	920	920	920	920
–O–SO$_3$ stretching at D-galactose-4-sulfate	839	–	842	842	842	842
Sulfate C-4 galactose	738		738	738	738	738
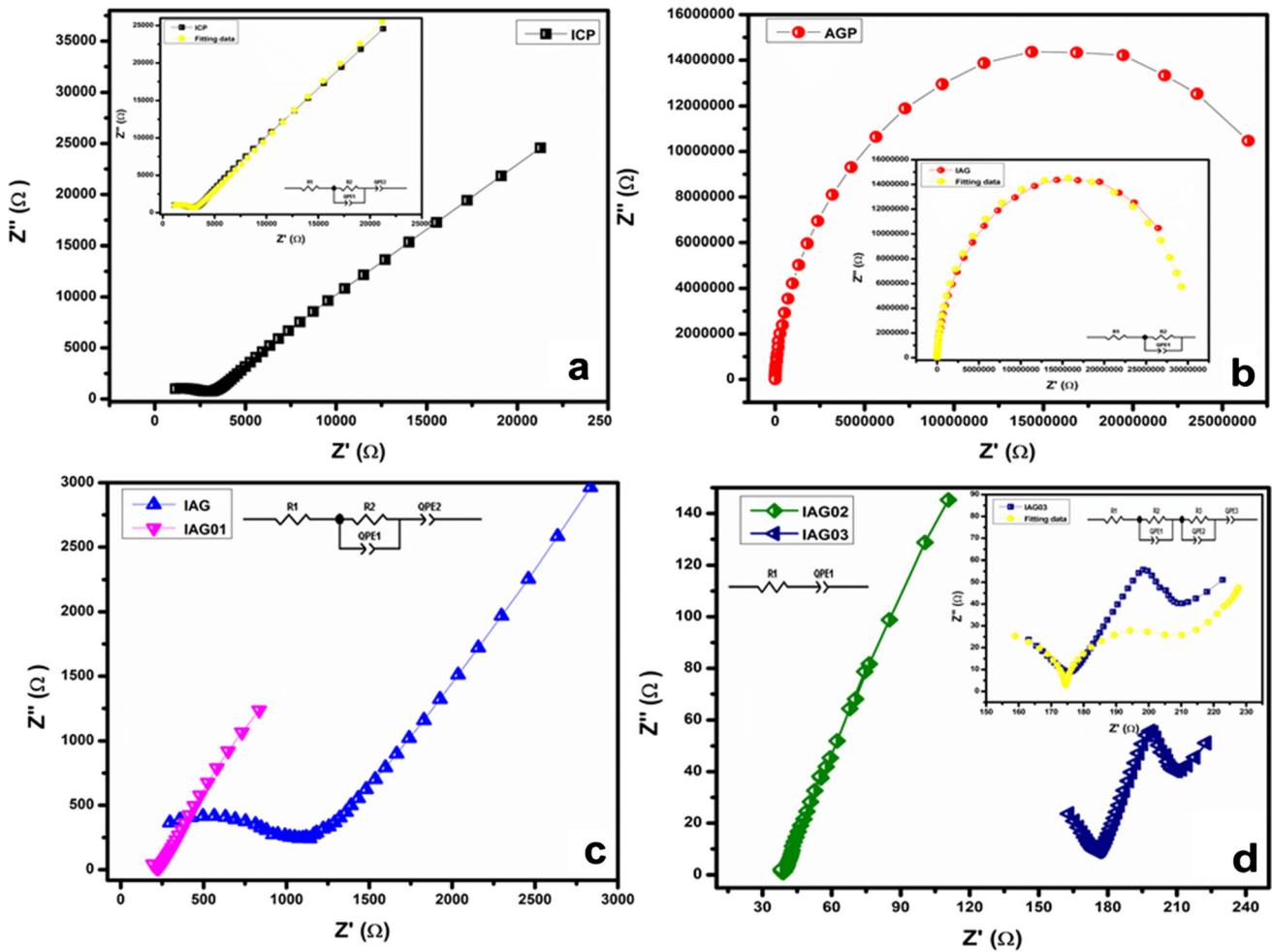
Fig. 4 Cole–Cole plot of ICP, AGP, IAG, and EG-added samples

bulk resistance[41]. The Nyquist plot shows the higher conductivity for the blend of IC and Gum Acacia with 0.75 ml EG (IAG02). For this electr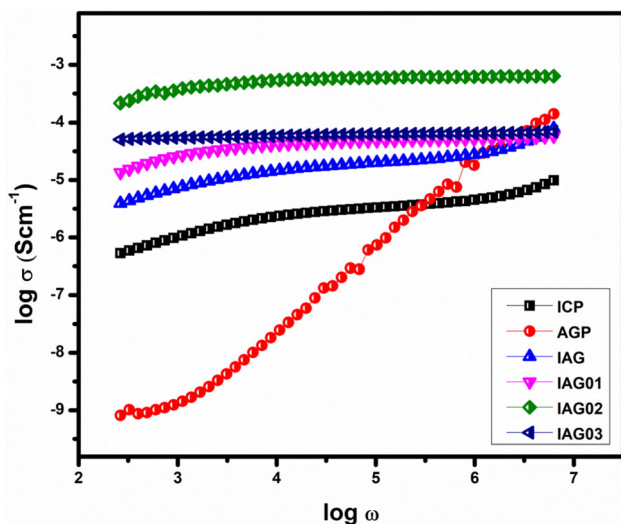olyte sample IAG02, the obtained conductivity value was 2.95×10^{-4} S cm^{-1} and 4.54×10^{-4} S cm^{-1} at 303 K and 348 K, respectively. This shows that the conductivity increases with the temperature.

Table 2 Calculated conductivity, activation energy values for ICP, AGP, IAG, IAG01, IAG02, and IAG03

Sample	Bulk resistance (Ω)	Conductivity (S cm^{-1})	Activation energy, E_a (eV)
ICP	2928	3.86×10^{-6}	0.14
AGP	26,445,807	4.91×10^{-10}	0.29
IAG	1080	4.77×10^{-6}	0.11
IAG01	231	4.90×10^{-5}	0.09
IAG02	40	2.96×10^{-4}	0.06
IAG03	220	4.93×10^{-5}	0.08

4.4 Conductivity studies

Figure 5 represents the conductance spectra which deliberates the ion kinetic and conductance behavior of all the prepared plasticized polymer blend electrolyte. AC conductivity counts on the equal sites of electrons and ions by relaxation, hopping, and tunneling. The figure depicts the conductivity as a function of log frequency for the pure IC, pure AG, and various concentrations of $C_2H_6O_2$ with blend polymer electrolytes [42]. Two different regions are obtained in the low-frequency dispersion region which is due to the space charge polarization along electrode interfacial and high-frequency plateau region. This frequency-independent plateau region corresponds to the σ_{dc} value [43]. In the high-frequency region, the σ_{dc} conductivity can be determined by extending the plateau region on the (log σ) y-axis. Conductivity value improves with the inclusion of $C_2H_6O_2$ into blend polymer system up to IAG02.

4.5 Temperature-dependent conductivity

Figure 6 explains the temperature dependence of ionic conductivity for ICP, AGP, IAG, IAG01, IAG02, and IAG03 samples over 303–353 K temperatures. The plot shows that the conductivity of the electrolyte is thermally activated process [41]. The conductivity value is enhanced with the addition of $C_2H_6O_2$ into the blend polymer electrolyte.

The activation energy (E_a) can be determined using the relationship between conductivity and temperature as follows:

$$\sigma = \sigma_o e^{\frac{-E_a}{k_b T}}, \tag{2}$$

where σ_o is the pre-exponential factor, k_b is the Boltzmann constant, and T is the temperature [44, 45]. Since the electrode and electrolyte interface polarization induces free electrons, that either promotes conduction, as the temperature increase, conductivity also increases. The calculated activation energy for the higher conducting sample is 0.06 eV, which is lower than the other samples [39, 46, 47].

Fig. 5 Conductance spectra of ICP, AGP, IAG, and EG-added samples
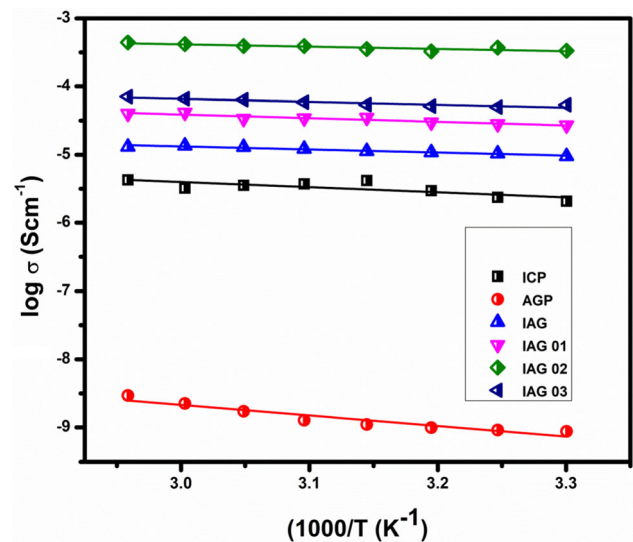

Fig. 6 Arrhenius plot for ICP, IAG, IAG01, IAG02, and IAG03

Table 2 shows the calculated activation energy with the corresponding conductivity values.

4.6 Conduction mechanism

The frequency-dependent conductivity is identified by two regions. One is the plateau region and the other is the dispersion region. Figure 7 shows the low-frequency plateau region due to space charge polarization for IAG02 sample at different temperatures and σ is independent of frequency [46]. Based on frequency exponent values, conductance response is given by the equations

$$\sigma(\omega, T) = \sigma_{dc} + \sigma_{ac}, \tag{3}$$

$$\sigma(\omega, T) = \sigma_{dc} + A(T)\omega^{s(T)}, \tag{4}$$

$$\omega^{s(T)} = (\sigma(\omega, T) - \sigma_{dc}), \tag{5}$$

$$\omega_H^{s(T)} = \frac{\sigma_{dc}}{A(T)}. \tag{6}$$

The power-law exponent s is generally less than unity. A is the temperature-dependent parameter $(A = \pi N^2 q^2 \alpha / 3kT)$ and ω_H is hopping frequency. Based on the above equations, higher conducting sample suppresses Jonscher power law [48, 49].

The conduction mechanism for the higher conducting sample is evaluated by frequency exponent (s) shown in Fig. 8. Various conduction mechanisms are used to identify the dynamics of charge carriers in each frequency interval based on the evolution of the frequency exponent (s) with T [50]. There is a number of models that explains the conduction mechanism
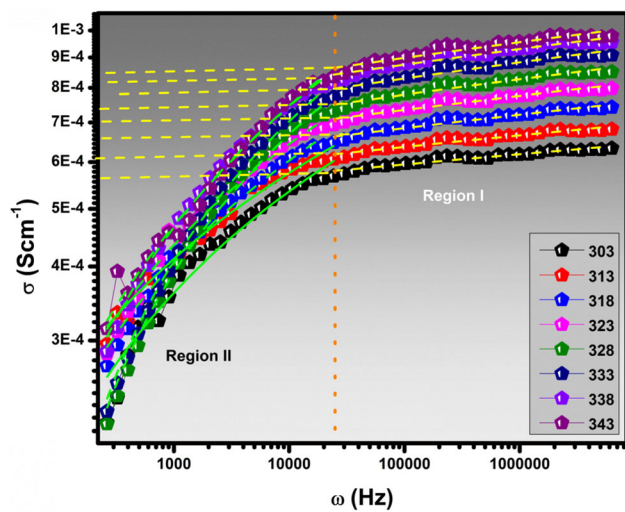

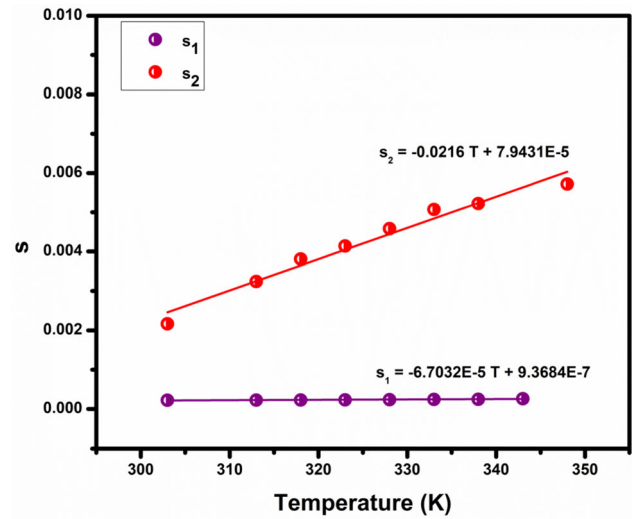Fig. 7 Conductance spectra for IAG02 at different temperatures

Fig. 8 The plot of power-law exponent s vs. temperature for higher conducting sample (IAG02)

those are quantum mechanical tunneling (QMT) model, the correlated barrier hopping (CBH) model, the overlapping large-polaron tunneling (OLPT) model, and the non-overlapping small polaron tunneling (NSPT) model. The frequency exponent (s) value is decreased with the increase in temperature and the exponent s is both frequency and temperature dependent obeying the OLPT conduction mechanism [51]. For IAG02, the exponent s_1 is to be independent of the temperature which represents the QMT model [52], and the exponent "s_2" increases with increasing temperature which confirms the activation of the NSPT mechanism in the high-frequency region [50, 53]. The corresponding fitting equation of higher conducting sample can be written as

$$s_1 = -0.0216T + 0.000079, \tag{7}$$

$$s_2 = -6.7032T + 0.00000094. \tag{8}$$

NSPT is performed when the new charge carrier is added to a site which makes localization of small polaron to exhibit a large degree of local lattice distortion [51].

4.7 Dielectric spectra

Figures 9 and 10 represent the dielectric constant (ε') and dielectric loss (ε'') as a function of logarithmic frequency for the prepared electrolytes. The recorded AC impedance data over the frequency range 42 Hz to 1 MHz at room temperature are utilized to obtain
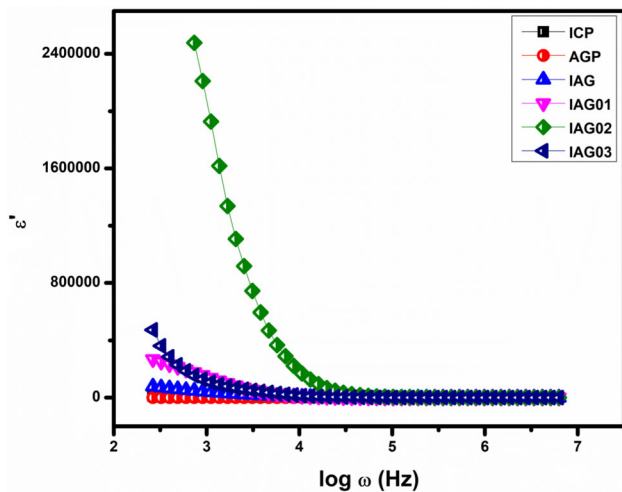
Fig. 9 Frequency vs. dielectric constant studies for ICP, AGP, IAG, and EG-added samples
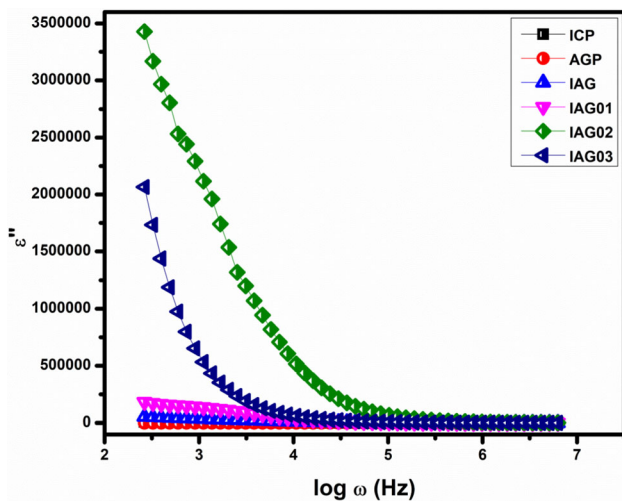

Fig. 10 Frequency vs. dielectric loss studies of ICP, AGP, IAG, and EG-added samples

the real and imaginary parts of energy storage by the following relation:

$$\varepsilon^*(\omega) = \varepsilon'(\omega) - i\varepsilon''(\omega), \tag{9}$$

$$\varepsilon'(\omega) = \frac{Z''}{\omega C_o(Z'^2 + Z''^2)}, \tag{10}$$

$$\varepsilon''(\omega) = \frac{Z'}{\omega C_o(Z'^2 + Z''^2)}, \tag{11}$$

where ε'' and ε' are the imaginary and real permittivity, ω is the angular frequency, Z' and Z'' represent the real and imaginary impedance, and C_o represents the vacuum capacitance. When the frequency is increased, the dielectric constant and loss (ε' and ε'')

decreases and become constant. This is because of the interruption of field and there is no way for the charge carriers to turn in the field's direction, as well as a lower amount of charge carrier dispersion in the field's direction [54]. Sample IAG02 has a larger dielectric constant at a lower frequency, which contributes to better dc conductivity than other samples [55].

The addition of $C_2H_6O_2$ to an optimized polymer electrolyte IAG enhances energy storage and loss. In the low-frequency domain, electrode polarization creates a large dielectric constant. The dielectric loss and constant increase with the addition of plasticizer to the blend polymer, whereas relaxation time decreases [22, 41].

4.8 Modulus spectra

Electrical behavior in the low-frequency band is provided by the AC impedance spectrum. Modulus studies offer additional insight into dielectric behavior and the electrical relaxation of ion-conducting lattices and measure the dispersal of ion energy. The real electrical modulus M' and imaginary electrical modulus M'' formulae are as follows:

$$M' = \frac{\varepsilon'}{\varepsilon'^2 + \varepsilon''^2}, \tag{12}$$

$$M'' = \frac{\varepsilon''}{\varepsilon'^2 + \varepsilon''^2}, \tag{13}$$

where M', M'' are the real and imaginary portions of the complex electric modulus [18, 49]. Because of the large capacitance values associated with electrodes, a long tail is evident in M' (approaching zero) in the low-frequency area for all electrolytes in Fig. 11a, c. The bulk effect is responsible for the progressive increase in modulus values as frequency rises [56, 57]. This backs up the non-Debye behavior of the samples. From Fig. 11b, d, the asymmetric curve shape is observed in M', M'' for AGP. The value of M', M'' increases with increasing frequency and reaches a maximum at higher frequencies without relaxation peaks, owing to the availability of relaxation processes over a wide frequency range [58].

4.9 Argond plot

The analysis of the Argond plot at various concentrations can demonstrate the idea of relaxation processes in polymer electrolytes. The Argond plot of
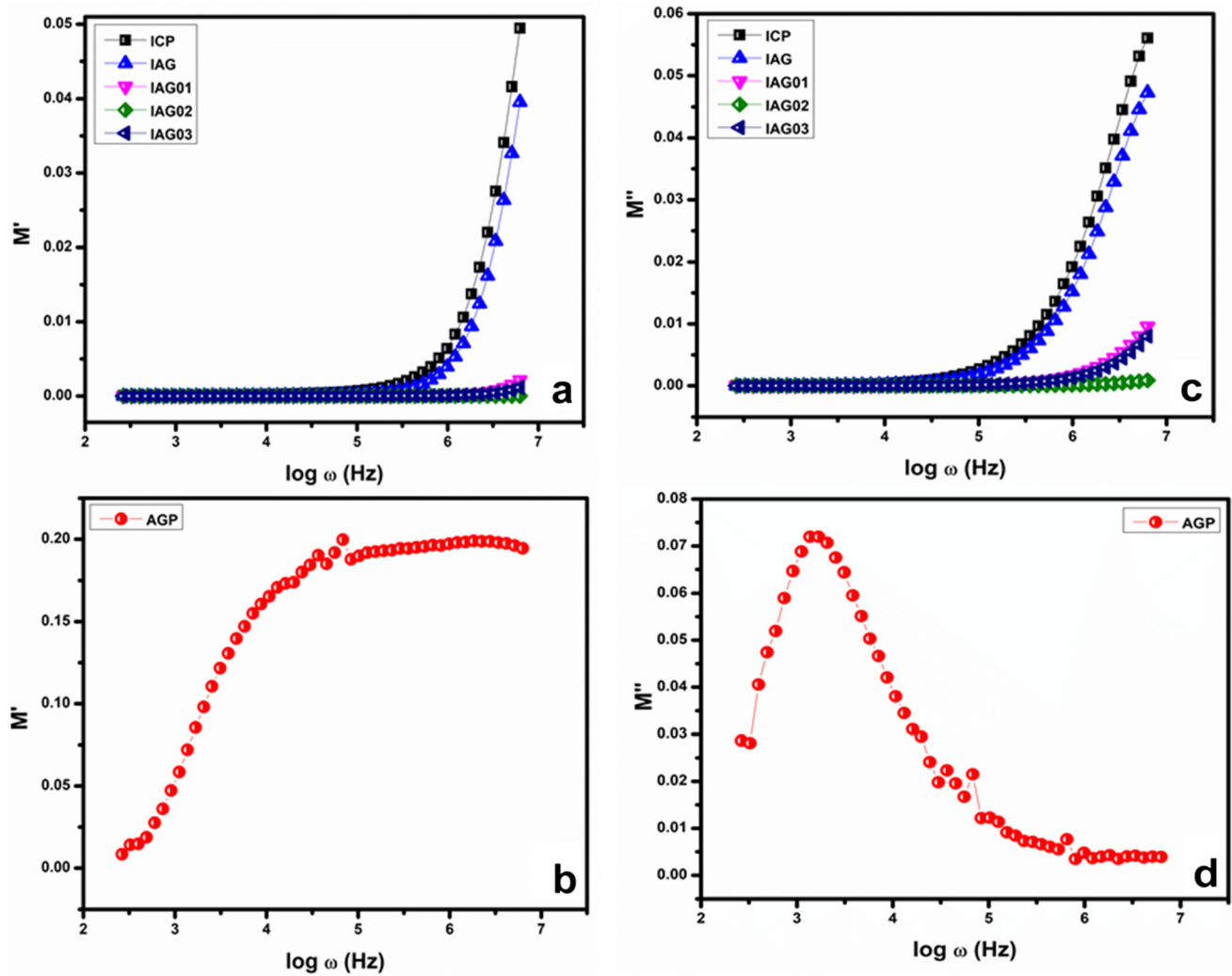
Fig. 11 Real and imaginary part of modulus spectra for ICP, AGP, IAG, and EG-added samples

ICP, AGP, IAG, IAG01, IAG02, IAG03 polymer electrolyte is shown in Fig. 12. The curves of the Argond plot show incomplete semicircles in Fig. 12a, suggesting non-Debye behavior. Due to an increase in plasticizer content in the polymer electrolyte, the radius of the semicircle arcs decreases. The relaxation time of the ions in polymer electrolytes is shortened when the radius of the semicircle arc is reduced [51]. The Argond plot of a higher conducting sample shows a small semicircle arc and a short relaxation time, contribute to the non-Debye character. The conductivity of the polymer electrolyte has a strong relationship with the arc radius [59].

4.10 Tangent spectra

At room temperature, Fig. 13 depicts the variation of tan δ with frequency for the prepared electrolytes. It has been discovered that when frequency increases, tan δ grows until it reaches a maximum value, after which it drops. With increasing salt content, the maximum of tan δ shifts to a higher frequency, and the height of the peak increases. This is due to an increase in the number of charge carriers available for conduction, which lowers the samples' resistivity [60]. The dielectric loss tangent delta can be defined by

$$\tan\delta = \frac{\varepsilon''}{\varepsilon'}. \tag{14}$$
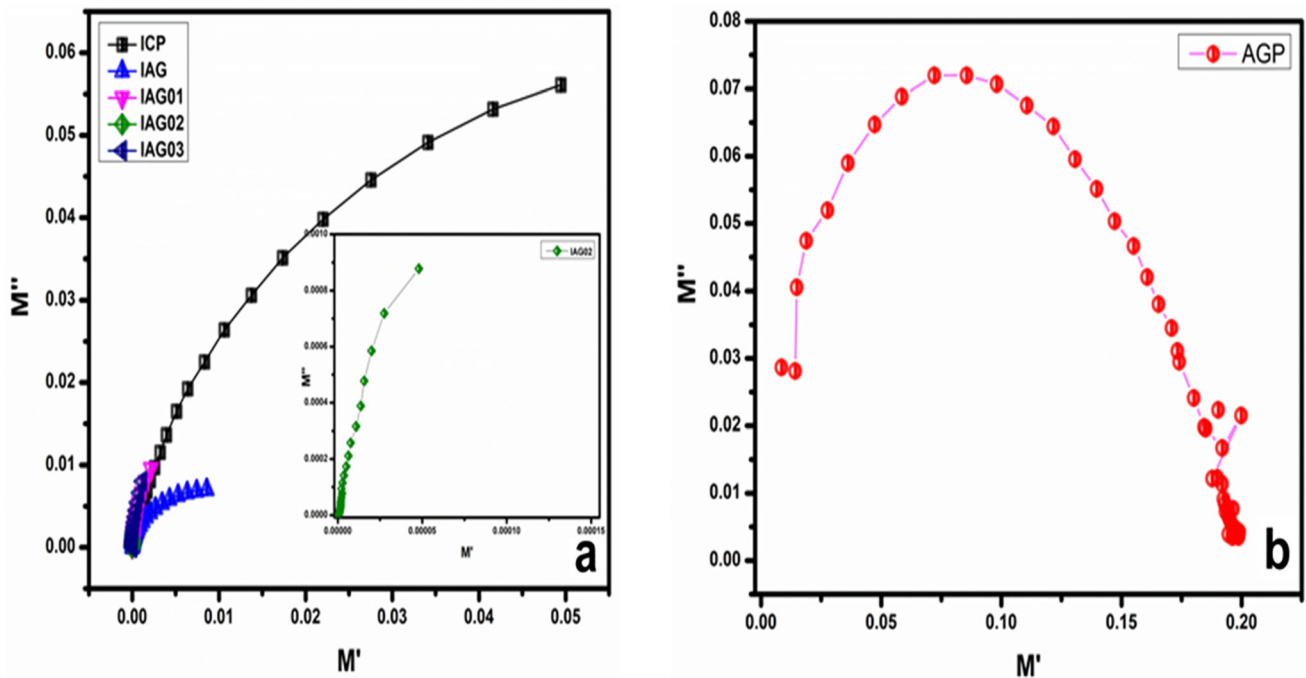
The loss tangent peak is expressed as

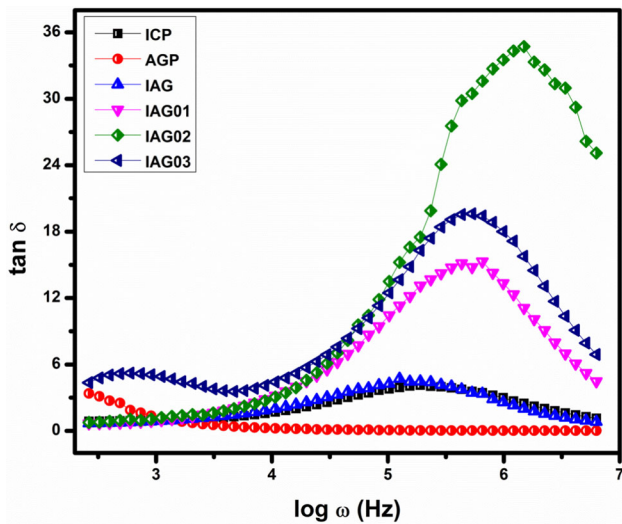**Fig. 12** Argond plot for ICP, AGP, IAG, and EG-added samples

Fig. 13 Tangent spectra for ICP, AGP, IAG, IAG01, IAG02, and IAG03

$$\omega\tau = 1, \tag{15}$$

$$\varphi(t) = \exp^{\left(-\frac{t}{\tau}\right)^{\beta}}, \tag{16}$$

$$\beta = 1.14/FWHM, \tag{17}$$

where ε'' represent imaginary part of dielectric, and ε' represent the real part of dielectric, τ and β are tangent relaxation time and the Kohlrausch exponent.

The higher conducting sample IAG02 attains a minimum relaxation time of 6.72×10^{-7} s. The FWHM exponent value of all prepared electrolytes is calculated based on the formula and listed in Table 3.

4.11 Cyclic voltammetry

CV is used to investigate the electrochemical behavior of polymer electrolytes, as well as redox processes, the presence of intermediates in redox reactions, and the stability of reaction products, electron transfer kinetics, and chemically reversible electron transfer is observed on the irreversibly adsorbed [51, 61]. At various scan rates, CV is performed in the potential window (0 to 1.4 V). For IAG02 electrolyte, CV curves are shown in Fig. 14. The intrinsic Faradaic reaction current of 50 mV s^{-1}

Table 3 Observed relaxation time and other parameters from tangent loss peak

Sample	Relaxation time, τ (s)	FWHM	β
ICP	5.08×10^{-6}	1.73	0.66
AGP	2.51×10^{-3}	3.53	0.32
IAG	7.93×10^{-6}	1.74	0.66
IAG01	1.53×10^{-6}	1.67	0.68
IAG02	6.72×10^{-7}	1.42	0.80
IAG03	1.88×10^{-6}	1.50	0.76
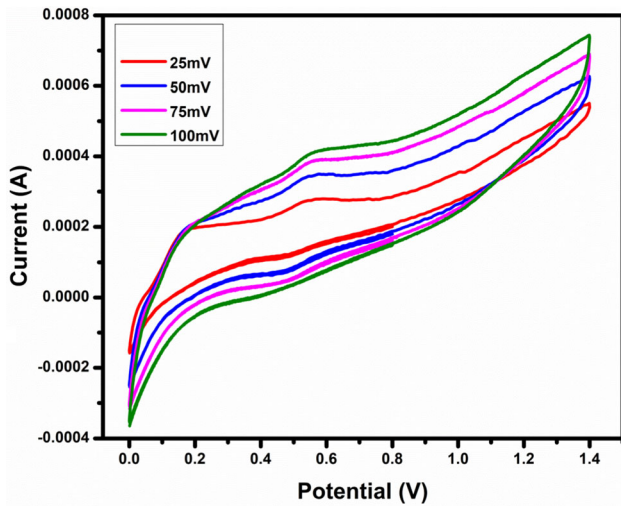
Fig. 14 Cyclic voltammetry curves of higher conducting sample IAG02

4.12 Linear sweep voltammetry (LSV)

For the prepared IAG02 electrolyte, LSV curves are shown in Fig. 15. In addition to high ionic conductivity, good electrochemical stability is essential for battery applications. LSV is observed using a two-electrode system with the configuration of SE∣∣∣∣AG02∣∣∣∣SE (silver electrode ∣∣∣∣ higher conducting electrolyte IAG02 ∣∣∣∣ silver electrode). This examination offers information about electrolyte's electrochemical stability. The electrochemical stability windows of 0.74 V are marked with an arrow, as shown in the plot of current vs. voltage [21, 64].

4.13 Optical properties

4.13.1 Absorbance spectra

By UV–Vis spectroscopy, optical properties like absorbance and transmittance are observed in the range of 200–800 nm [65]. Optical absorbance and absorbance coefficient Spectra of the SPE are shown in Fig. 16. The variation in the optical energy bandgap (E_g) is due to the transition of the amorphous nature of the material. In this SPE, the absorbance peak appears as a single peak and is well-defined in the wavelength range from 200 to 220 nm [66]. This peak is assigned to n–π* transition [67]. While increasing the concentration of EG with the blend of Iota-Carrageenan and Gum Acacia, the absorbance

is significantly higher than the low scan rate reaction current. All scan rates of 25 mV s^{-1}, 50 mV s^{-1}, 75 mV s^{-1}, and 100 mV s^{-1} in CV curves show two distinct small symmetric peaks in the positive scans, indicating the remarkable reversibility of Faradaic responses. As the scan rate rises, the redox peaks rise with it. The ions migration is enhanced by raising the scan rate. Since the resistance is reduced, resulting in an increase in the area of the electrolyte's CV graph [60, 62, 63].
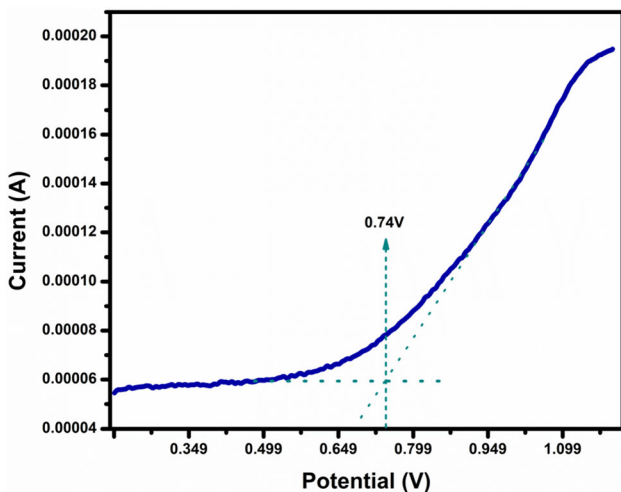

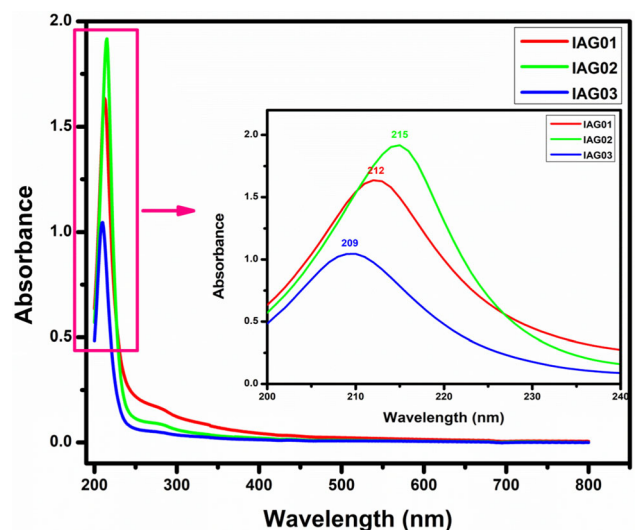Fig. 15 Linear sweep voltammetry studies of IAG02 electrolyte

Fig. 16 UV-spectra of IAG01, IAG02, and IAG03

peak also increases. In Fig. 17, the absorbance coefficient of the SPE depends on the material and wavelength of the light passed through it.

Absorbance coefficient is defined as

$$\alpha = (\ln T)/t, \tag{18}$$

whereas 'T' is the transmittance and 't' is the thickness of the sample. Using this absorbance coefficient with photon energy, we can easily calculate the optical bandgap energy [21].

4.13.2 Transmittance spectra

Figure 18 represents the transmittance spectra of the various amount of EG-added polymer electrolyte films. The films are transparent in the visible region. The transmittance increases with the addition of EG from the range of 220 nm [68]. Beer–Lambert's law states that there is a linear relationship between the concentration of the sample and the transmittance.

4.13.3 Optical bandgap energy

The absorbance coefficient is used for the determination of the optical bandgap energy (E_g). It is expressed by Tauc's plot,

$$\alpha h v = A\left(h v - E_g\right)^n. \tag{19}$$

Here, 'α' is the absorbance coefficient, 'hv' is the photon energy, 'A' is constant, and 'n' depends on the type of transition. The type of electronic transitions
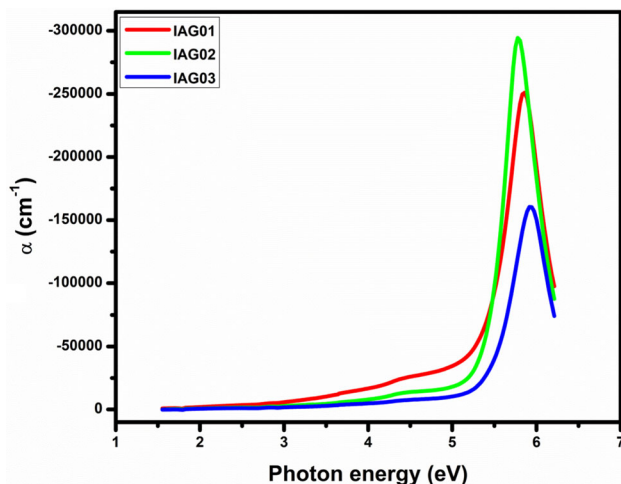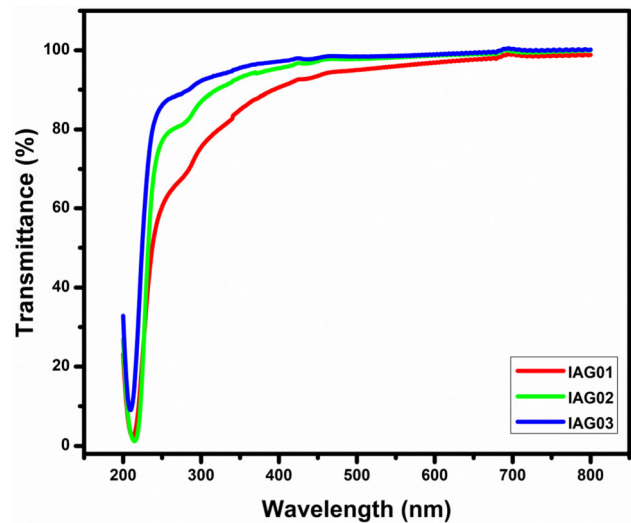

Fig. 18 Transmittance spectra of IAG01, IAG02, and IAG03

that cause optical absorption is determined by the value of n, which can be 1/2, 3/2, 2, or 3 for direct-allowed, direct-forbidden, indirect-allowed, and indirect-forbidden transitions, respectively. Tauc's plot for indirect bandgap plotted between hv and $(\alpha h v)^2$, the intersections of the resulting straight lines with the energy axis at $(\alpha h v)^2 = 0$ can be used to determine the direct optical energy gap [69]. From Fig. 19, the optical bandgap energy E_g is calculated and it seems to decrease while increasing the percentage of EG. For the samples IAG01 and IAG03, bandgap energy attains the value of 5.38 eV and 5.55 eV, respectively. IAG02, higher conducting electrolyte, has bandgap energy of 5.31 eV [70]. Figure 20 shows the direct bandgap graph of hv and $(\alpha h v)^{(1/2)}$. For plasticizer-added samples direct

Fig. 17 The absorbance coefficient of the depends on different concentration of EG-added electrolytes
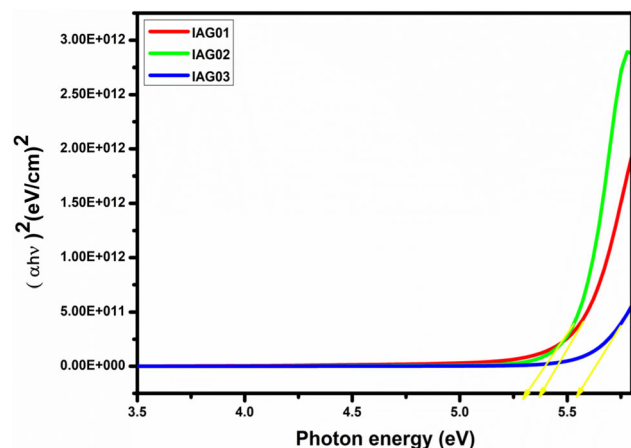

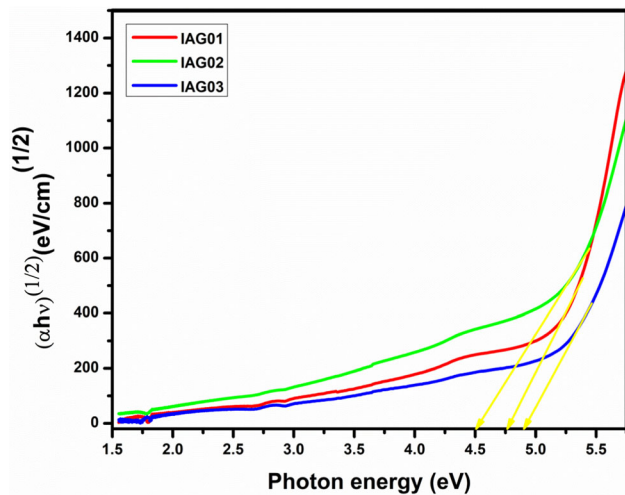Fig. 19 Indirect bandgap (Tauc plot) for IAG01, IAG02, and IAG03

Fig. 20 Direct bandgap (Tauc plot) for IAG01, IAG02, and IAG03

bandgap lies at 4.52 eV, 4.16 eV, and 4.73 eV for IAG01, IAG02, and IAG03 correspondingly. Similarly, from Fig. 21 it is observed that the optical dielectric bandgap values for IAG01, IAG02, and IAG03 are 5.65 eV, 5.54 eV, and 5.72 eV. To identify the dominant electronic transition, the observed bandgap energy based on Tauc's method was compared with optical dielectric bandgap energy values [69, 71, 72]. From these figures optical bandgap was estimated and tabulated in Table 4. As the result of comparison indirect bandgap ($n = 2$) was concluded for the prepared electrolytes.
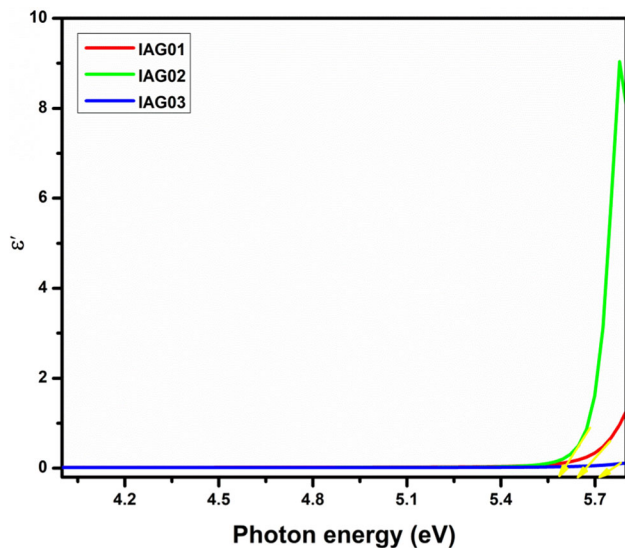

Fig. 21 Optical dielectric plot of plasticizer-added samples
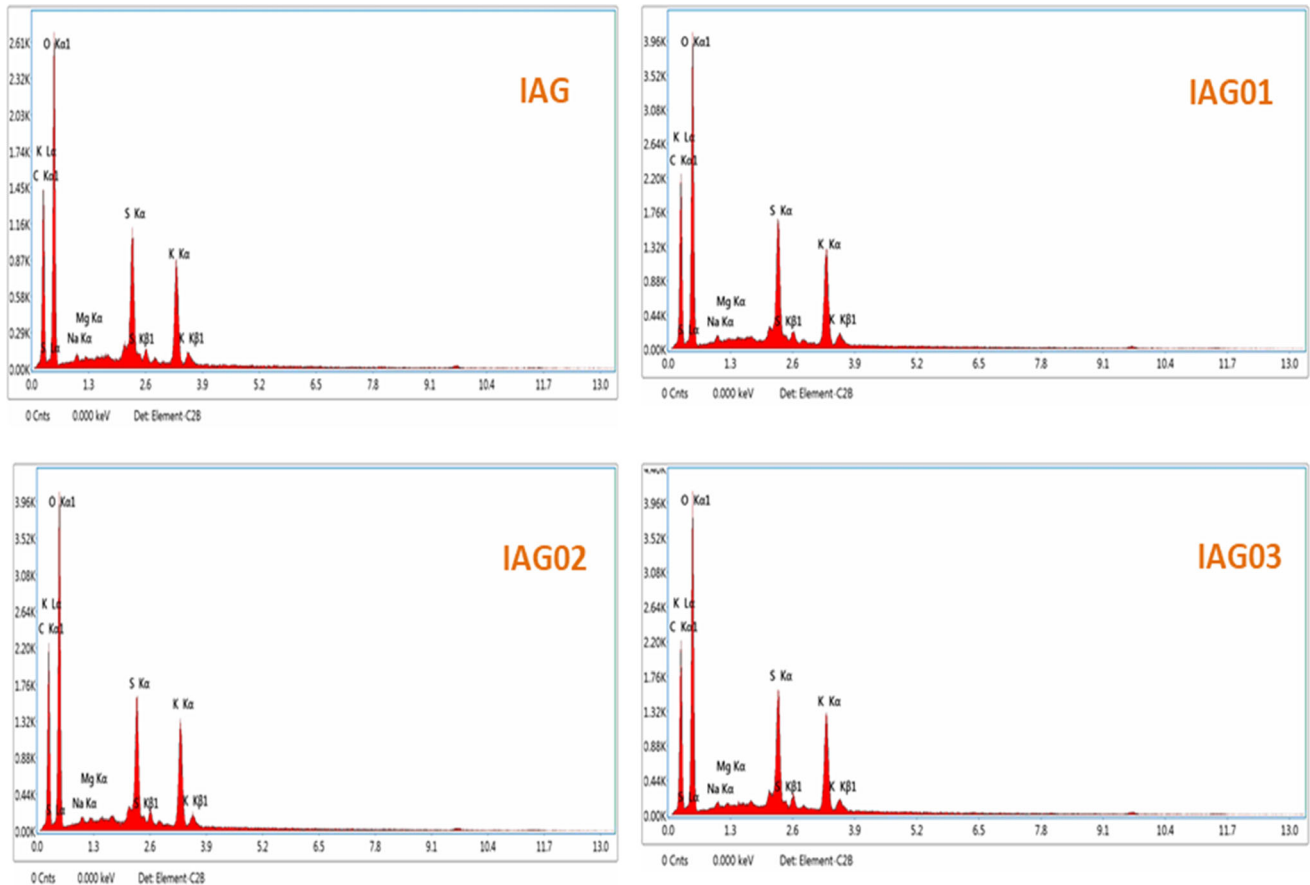
5 Energy-dispersive spectroscopy (EDS)

Energy-dispersive X-ray spectroscopy (EDS) was done for the samples to confirm the elements present in the prepared electrolytes. The elemental conformation EDS spectrum is shown in Fig. 22. The only peaks corresponding to the following elements such as O, C, S, K, Mg, and Na appeared and no other impurity peaks (Ca) were noted.

6 Conclusions

The solution casting method has been used to develop biopolymer electrolytes based on IC and AG with different concentrations of EG. The XRD pattern of all the prepared samples shows that the inclusion of EG in the polymer blend diminishes the intensity of the peak and thereby decreases the amorphous nature of the polymer electrolytes. The presence of functional groups in the FTIR study exposes the addition of $C_2H_6O_2$ which results from the wavenumber shifts. EDX result confirms the presence of the elements in the electrolytes. Using Zsimp win software, impedance plot of all the prepared samples fitted with equivalent circuit. Impedance study reveals the decrease in resistance value with the inclusion of EG. The sample IAG02 seems to have higher conductivity of 2.96×10^{-4} S cm^{-1}. From the result of dielectric studies, the rise in the temperature, the dielectric permittivity, and the loss increases for all samples. Modulus studies have revealed the consequences of electrode polarization. The relaxing process is explained using an Argond plot. The tangent loss point of higher conducting sample is used to estimate the relaxation time (τ), FWHM, which is 6.72×10^{-7} s, 1.42, and 0.80 correspondingly. The minimum bandgap value of IAG02 is found to be 5.31 eV after studying the optical characteristics of the electrolytes. This confirms the minimum bandgap of higher conducting sample. The CV investigation revealed the Faradic behavior of this higher conducting sample. LSV result shows the stability of the higher conducting electrolyte. Based on all the studies, this environmentally friendly and cost-effective bio-based electrolyte could be used in energy storage devices.

Table 4 Bandgap energy comparison for IAG01, IAG02, and IAG03

Sample	Direct bandgap $n = 1/2$ (eV)	Indirect bandgap $n = 2$ (eV)	Dielectric bandgap (eV)
IAG01	4.52	5.38	5.65
IAG02	4.16	5.31	5.54
IAG03	4.73	5.55	5.72

Fig. 22 Energy-dispersive X-ray spectroscopy (EDX) for IAG, IAG01, IAG02, and IAG03

Author contributions

All authors contributed to the study conception and design. Material preparation, data collection, and analysis were performed by MN. The first draft of the manuscript was written by DV and all authors commented on the previous versions of the manuscript. All authors read and approved the final manuscript.

Funding

Data availability

The datasets generated during and/or analyzed during the current study are available from the corresponding author on reasonable request.

Declarations

Conflict of interest　On behalf of all authors, the corresponding author states that there is no conflict of interest.

References

1. S. Ahmad, Ionics (Kiel) **15**, 309 (2009)

2. M. Rayung, M.M. Aung, S.C. Azhar, L.C. Abdullah, M.S. Su'ait, A. Ahmad, S.N.A.M. Jamil, Materials (Basel) **13**(1), 47 (2020)

3. A.S. Samsudin, E.C.H. Kuan, M.I.N. Isa, Int. J. Polym. Anal. Charact. **16**, 477 (2011)

4. S. Ramesh, C.W. Liew, A.K. Arof, J. Non-cryst, Solids **357**, 3654 (2011)

5. M. Muthukrishnan, C. Shanthi, S. Selvasekarapandian, R. Manjuladevi, P. Perumal, P. Chrishtopher Selvin, Ionics (Kiel) **25**, 203 (2019)

6. A.K.A.S.R. Majid, Physica B **355**, 78 (2005)

7. S. Selvalakshmi, T. Mathavan, S. Selvasekarapandian, M. Premalatha, Ionics (Kiel) **24**, 2209 (2018)

8. H. Rajeswari, S.L. Jagadeesh, G.J. Suresh, J. Nutr. Health Food Eng. **8**, 487 (2018)

9. M. Almoiqli, A. Aldalbahi, M. Rahaman, P. Govindasami, S. Alzahly, Polymers (Basel) **10**(1), 14 (2018)

10. N.K. Zainuddin, A.S. Samsudin, Mater. Today Commun. **14**, 199 (2018)

11. C. Tranquilan-Aranilla, N. Nagasawa, A. Bayquen, A. Dela Rosa, Carbohydr. Polym. **87**, 1810 (2012)

12. A.S. Samsudin, W.M. Khairul, M.I.N. Isa, J. Non-cryst. Solids **358**, 1104 (2012)

13. P. Sangeetha, T.M. Selvakumari, S. Selvasekarapandian, S.R. Srikumar, R. Manjuladevi, M. Mahalakshmi, Ionics (Kiel) **26**, 233 (2020)

14. N.S. Mohamed, S. Rudhziah, N.A.C. Apandi, R.H.Y. Subban, Sci. Lett. **12**, 45 (2018)

15. A.N. Al-Baarri, A.M. Legowo, H. Rizqiati, Widayat, A. Septianingrum, H.N. Sabrina, L.M. Arganis, R.O. Saraswati, R.C.P.R. Mochtar, IOP Conf. Ser. Earth Environ. Sci. **102**, 012056 (2018)

16. N.A.A. Ghani, R. Othaman, A. Ahmad, F.H. Anuar, N.H. Hassan, Arab. J. Chem. **12**, 370 (2019)

17. J. Necas, L. Bartosikova, Vet. Med. (Praha) **58**, 187 (2013)

18. A.K. Arof, N.E.A. Shuhaimi, N.A. Alias, M.Z. Kufian, S.R. Majid, J. Solid State Electrochem. **14**, 2145 (2010)

19. A. Pawlicka, F.C. Tavares, D.S. Dörr, C.M. Cholant, F. Ely, M.J.L. Santos, C.O. Avellaneda, Electrochim. Acta **305**, 232 (2019)

20. E.M.I. Elzain, A.A. Mariod, 8—Analytical techniques for new trends in gum arabic (GA) research, in *Gum Arabic* (Elsevier, Inc., Amsterdam, 2018).

21. R. Shilpa, R. Saratha, AIP Conf. Proc. **2270**, 100006 (2020)

22. I. Jenova, K. Venkatesh, S. Karthikeyan, S. Madeswaran, G. Aristatil, P. Moni, J. Solid State Electrochem. **25**, 2371 (2021)

23. I.S.M. Noor, S.R. Majid, A.K. Arof, D. Djurado, S. Claro Neto, A. Pawlicka, Solid State Ion. **225**, 649 (2012)

24. P. Grewal, J. Mundlia, M. Ahuja, Carbohydr. Polym. **209**, 400 (2019)

25. B. Gaida, A. Brzęczek-Szafran, Molecules **25**(1), 24 (2020)

26. S.B. Aziz, M.M. Nofal, R.T. Abdulwahid, M.F.Z. Kadir, J.M. Hadi, M.M. Hessien, W.O. Kareem, E.M.A. Dannoun, S.R. Saeed, Results Phys. **29**, 104770 (2021)

27. S.B. Aziz, E.M.A. Dannoun, R.T. Abdulwahid, M.F.Z. Kadir, M.M. Nofal, S.I. Al-Saeedi, A.R. Murad, Membranes (Basel) **12**(1), 21 (2022)

28. M.N. Chai, M.I.N. Isa, Int. J. Polym. Anal. Charact. **18**, 280 (2013)

29. M.N. Chai, M.I.N. Isa, Nat. Publ. Gr. **6**, 1–7 (2016)

30. S. Ramesh, A.K. Arof, Mater. Sci. Eng. **85**, 11 (2001)

31. R. Chitra, P. Sathya, S. Selvasekarapandian, S. Meyvel, Polym. Bull. **77**, 1555 (2020)

32. M. Khalid, A.M.B. Honorato, J. Solid State Electrochem. **21**, 2443 (2017)

33. C.M. Cholant, L.U. Krüger, R.D.C. Balboni, M.P. Rodrigues, F.C. Tavares, L.L. Peres, W.H. Flores, A. Gündel, A. Pawlicka, C.O. Avellaneda, Ionics (Kiel) **26**, 2941 (2020)

34. M. Raman, V. Devi, M. Doble, J. Nanobiotechnol. **13**, 1 (2015)

35. F.N. Jumaah, N.N. Mobarak, A. Ahmad, M.A. Ghani, M.Y.A. Rahman, Ionics (Kiel) **21**, 1311 (2015)

36. S. Shanmuga Priya, M. Karthika, S. Selvasekarapandian, R. Manjuladevi, S. Monisha, Ionics (Kiel) **24**, 3861 (2018)

37. S. Karthikeyan, S. Selvasekarapandian, M. Premalatha, S. Monisha, G. Boopathi, G. Aristatil, A. Arun, S. Madeswaran, Ionics (Kiel) **23**, 2775 (2017)

38. C.M. Cholant, M.P. Rodrigues, L.L. Peres, R.D.C. Balboni, L.U. Krüger, D.N. Placido, W.H. Flores, A. Gündel, A. Pawlicka, C.O. Avellaneda, J. Solid State Electrochem. **24**, 1867 (2020)

39. T. Sugumaran, D.S. Silvaraj, N.M. Saidi, N.K. Farhana, S. Ramesh, K. Ramesh, S. Ramesh, Ionics (Kiel) **25**, 763 (2019)

40. A.S.F.M. Asnawi, S.B. Aziz, I. Brevik, M.A. Brza, Y.M. Yusof, S.M. Alshehri, T. Ahamad, M.F.Z. Kadir, Polymers (Basel) **13**, 1 (2021)

41. K. Sundaramahalingam, S. Jayanthi, D. Vanitha, N. Nallamuthu, Ionics (Kiel) **27**, 3919 (2021)

42. M.S.A. Rani, N.A. Dzulkurnain, A. Ahmad, N.S. Mohamed, Int. J. Polym. Anal. Charact. **20**, 250 (2015)

43. V. Moniha, M. Alagar, S. Selvasekarapandian, B. Sundaresan, G. Boopathi, J. Non-cryst. Solids **481**, 424 (2018)

44. N.S. Salleh, S.B. Aziz, Z. Aspanut, M.F.Z. Kadir, Ionics (Kiel) **22**, 2157 (2016)

45. V. Duraikkan, A.B. Sultan, N. Nallaperumal, A. Shunmuganarayanan, Ionics (Kiel) **24**, 139 (2018)

46. R. Punia, R.S. Kundu, M. Dult, S. Murugavel, N. Kishore, R. Punia, R.S. Kundu, M. Dult, S. Murugavel, N. Kishore, J. Appl. Phys. **112**, 083701 (2012)

47. Z. Imran, M.A. Rafiq, M. Ahmad, K. Rasool, S.S. Batool, M.M. Hasan, AIP Adv. **3**, 1 (2013)

48. P. Singh, O. Parkash, D. Kumar, Phys. Rev. B **84**, 174306 (2011)

49. Y. Moualhi, M.M. Nofal, R. M'nassri, H. Rahmouni, A. Selmi, M. Gassoumi, K. Khirouni, A. Cheikrouhou, Ceram. Int. **46**, 1601 (2020)

50. Y. Moualhi, R. M'nassri, H. Rahmouni, RSC Adv. **10**, 33868 (2020)

51. N. Nallamuthu, M. Manikandan, A. Anandha Jothi, D. Vanitha, S. Asath Bahadur, Physica B **580**, 411940 (2020)

52. Y.M. Yusof, M.F. Shukur, H.A. Illias, M.F.Z. Kadir, Phys. Scr. **89**, 035701 (2014)

53. S. Nasri, M. Megdiche, M. Gargouri, Ceram. Int. **42**, 943 (2016)

54. R. Chitra, P. Sathya, S. Selvasekarapandian, S. Meyvel, Mater. Res. Express **7**, 015309 (2019)

55. A.M.A. Nada, M. Dawy, A.H. Salama, Mater. Chem. Phys. **84**, 205 (2004)

56. M. Nandhinilakshmi, D. Vanitha, N. Nallamuthu, M. Anandha Jothi, K. Sundaramahalingam, Polym. Bull. (2022). https://doi.org/10.1007/s00289-022-04230-1

57. M. Nandhinilakshmi, D. Vanitha, N. Nallamuthu et al. J. Mater. Sci: Mater. Electron. **33**, 12648–12662 (2022)

58. G. Boopathi, S. Pugalendhi, S. Selvasekarapandian, M. Premalatha, S. Monisha, G. Aristatil, Ionics (Kiel) **23**, 2781 (2017)

59. K. Sundaramahalingam, D. Vanitha, N. Nallamuthu, A. Manikandan, M. Muthuvinayagam, Physica B **553**, 120 (2019)

60. N. Rajeswari, S. Selvasekarapandian, C. Sanjeeviraja, J. Kawamura, S. Asath Bahadur, Polym. Bull. **71**, 1061 (2014)

61. S.H. DuVall, R.L. McCreery, Anal. Chem. **71**, 4594 (1999)

62. S. Ramesh, N. Farah, H.M. Ng, A. Numan, C.-W. Liew, N.A.A. Latip, K. Ramesh, Mater. Sci. Eng. B **251**, 114468 (2019)

63. B. Jinisha, K.M. Anilkumar, M. Manoj, P. Pradeep, J. Jayalekshmi, Electrochim. Acta **235**, 210 (2017)

64. P.B. Bhargav, V.M. Mohan, A.K. Sharma, Ionics (Kiel) **13**, 441 (2007)

65. M. Irfan, A. Manjunath, S.S. Mahesh, R. Somashekar, T. Demappa, J. Mater. Sci. Mater. Electron. **32**, 5520 (2021)

66. A. Slistan-Grijalva, R. Herrera-Urbina, J.F. Rivas-Silva, M. Ávalos-Borja, F.F. Castillón-Barraza, A. Posada-Amarillas, Mater. Res. Bull. **43**, 90 (2008)

67. E.M. Abdelrazek, I.S. Elashmawi, S. Labeeb, Physica B **405**, 2021 (2010)

68. S.K.S. Basha, G.S. Sundari, K.V. Kumar, M.C. Rao, J. Inorg. Organomet. Polym. Mater. **27**, 455 (2017)

69. S.B. Aziz, A.Q. Hassan, S.J. Mohammed, W.O. Karim, M.F.Z. Kadir, H.A. Tajuddin, N.N.M.Y. Chan, Nanomaterials **9**, 216 (2019)

70. S. Krishnan, C.J. Raj, S. Dinakaran, R. Uthrakumar, R. Robert, S.J. Das, J. Phys. Chem. Solids **69**, 2883 (2008)

71. M. Arasakumari, K Subramanian, Res. Sq. (2021). https://doi.org/10.21203/rs.3.rs-589123/v1

72. U. Sasikala, P.N. Kumar, V.V.R.N. Rao, A.K. Sharma, Int. J. Eng. Sci. Adv. Technol. **2**, 722 (2012)